Geothermics 57 (2015) 95–103

Contents lists available at ScienceDirect

Geothermics

journal homepage: www.elsevier.com/locate/geothermics

Modeling and experimental validation of a transient direct expansion geothermal heat exchanger

Clément Rousseau [a,*], Jean-Louis Comlan Fannou [a], Louis Lamarche [a], Mohamed Ouzzane [b], Stanislaw Kajl [a]

[a] École de technologie supérieure, Montréal, Canada
[b] CanmetENERGY, Varenne, Canada

ARTICLE INFO

Article history:
Received 8 April 2014
Received in revised form 26 May 2015
Accepted 10 June 2015

Keywords:
Direct expansion geothermal heat pump
Ground exchanger
Modeling
R22

ABSTRACT

Geothermal heat pump technology is currently one of the most interesting technologies used to heat buildings. There are two designs used in the industry: geothermal heat pump using a secondary ground loop and direct expansion (DX) ground source heat pump. The latter is less used, with one of the possibly reasons being that less research has carried out into the design of this sort of heat pump. In this paper, a model of a ground heat exchanger of a DX geothermal heat pump is presented in heating mode and a comparison with experimental results is presented. It is shown that the model is adequately validated by our experiment. After this validation, an analysis of the effect of the mass flow rate, the length and the angle of the borehole on the heat flux rate is presented. To conclude, an optimum configuration for the experiment is proposed.

1. Introduction

The last decade has seen a jump in interest in the geothermal heat pump (GHP). This may be explained by the fact that this technology can provide heating and cooling for a building at very low cost. There are two designs used in the industry, namely, the geothermal heat pump using a secondary ground loop and the direct expansion (DX) ground source heat pump. Both operate on the simple vapour compression refrigeration cycle (Beauchamp et al., 2013), with the main difference between them being that with the DX geothermal heat pump (Fig. 1), the ground heat exchanger is part of the refrigeration cycle. The energy and operational performances of the system are thus directly related to the working fluid behavior, the refrigerant, in relation with the ground heat transfer.

A review of the literature reveals the presence of several publications on geothermal secondary loop systems (Capozza et al., 2012; Esen and Inalli, 2009; Self et al., 2013), but a lack of scientific research and publications on direct expansion geothermal heat pump systems. One of the first studies of the DX heat pump was conducted by Smith (1956), who studied a geothermal DX horizontal heat pump and compared it to a secondary loop heat system. He proved that the size of the exchanger can be reduced, but also that the heat rejection or heat absorption needs to be controlled according to changes in ground temperature. One problem he encountered was in controlling the oil in the ground exchanger. Following this study, many other research endeavors also arrived at the same conclusion (Freund and Whitlow, 1959; Goulburn and Fearon, 1978, 1983).

More recently, a few works have been published on DX heat pumps. Wang et al. (2009) conducted an experimental study of a DX heat pump with the refrigerant R134a in heating mode. Their system consisted of three vertical 30 m deep boreholes examined over a period of 20 days in the winter. According to the results, on average, COP_{hp} and COP_{sys} were 3.55 and 2.28, respectively, and the average heating capacity obtained was 6.43 kW. They noted the problem of maldistribution of refrigerant flow between the boreholes. Wang et al. (2013) conducted an experimental study on a DX heat pump in heating mode, consisting of four vertical 20 m wells for which a copper coil system was developed to facilitate oil return. Fannou et al. (2014) analyzed an experiment with three vertical 30 m deep boreholes in heating mode like Wang et al., but with R22. They concluded that a dimensioning effort should be made to minimize pressure drop in the evaporator in order to find a compromise between low pressure drop, oil return and refrigerant charge. In 2011, Halozan (2011) presented a study on the commercialization of ground source heat pumps and the barriers facing the technology, in which he highlighted the lack of a

* Corresponding author at: 1100 Notre-Dame Street West, Montréal, Quebec H3C 1K3, Canada. Tel.: +1 514 209 1761.
E-mail address: clement.rousseau.2@ens.etsmtl.ca (C. Rousseau).

http://dx.doi.org/10.1016/j.geothermics.2015.06.007
0375-6505/

Nomenclature

A	internal section of the pipe (m^2)
c_p	specific heat (J/kg K)
D_e	external diameter of the pipe (m)
D_i	internal diameter of the pipe (m)
D_b	extern diameter of the borehole (m)
f	friction factor
G	mass flux (kg/s m^2)
g	gravitational acceleration (m/s^2)
H_r	heat transfer coefficient between the pipe and the flow (W/m^2 K)
H_s	heat transfer coefficient, between the pipe and the grout (W/m^2 K)
H_p	heat transfer coefficient, between the grout and the ground (W/m^2 K)
h	specific enthalpy (J/kg)
h_{fg}	Enthalpy of phase changes (J/kg)
k	thermal conductivity (W/m K)
L	length of the pipe (m)
$\dot{m}$	mass flow rate (kg/s)
v	speed of the R22 (m/s)
P	pressure (Pa)
Pr	Prandtl number
Re	Reynolds number
R	Rayon (m)
T	temperature (K)
t	time (s)
x	quality of vapour (m)
z	depth

Greek letters

ρ	density (kg/m^3)
μ	dynamic viscosity (Pa s)
θ	angle of the pipe compared to the horizontal
σ	surface tension (N/m)
τ	shear stress (Pa)

Subscripts

c	grout
f	liquid phase
g	gas phase
m	mixture of liquid and gas of R22
p	pipe
s	ground
i	at the entry of the evaporator

design method as one of the major problems facing DX technology.

The proposed modeling and analysis of this DX heat pump therefore aims to fill this gap. The modeling and analysis of a direct expansion geothermal heat pump begins with the modeling of different components: ground heat exchanger, compressor, thermostatic expansion valve, reversing valve, pipe, and water-refrigerant exchanger, and the coupling of these components to form a closed loop corresponding to the heat pump.

The first step of the research, the modeling of the ground heat exchanger in evaporator mode, is presented in this paper.

We present a model of the ground exchanger operating like an evaporator in 1 dimension (Fig. 2). The model represents the phase change of the refrigerant, here Chlorodifluoromethane R22, with governing continuity, momentum and energy equations, and with heat exchange between the pipe and the grout and between the grout and the ground.

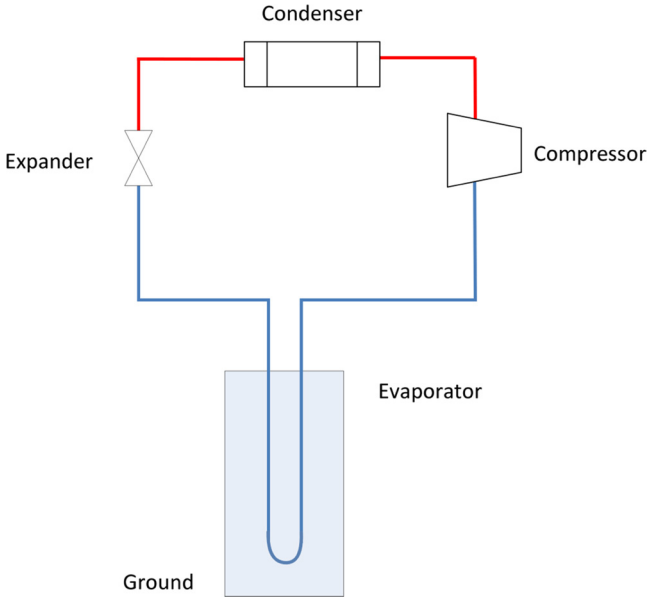

Fig. 1. Direct expansion heat pump.

To take the effect of the tube between them into account, two flows are created, one for the ascending flow, and one for the descending flow.

2. Theory

In this study, the equations of governing continuity, momentum and energy and heat exchange between the flow and the pipe, the pipe and the grout, and finally, the grout and the ground, are solved, Fig. 3.

The model is devised into four domains:

- The flow of R22, ascending and descending, in one dimension (z);
- The pipe, ascending and descending, in one dimension (z);

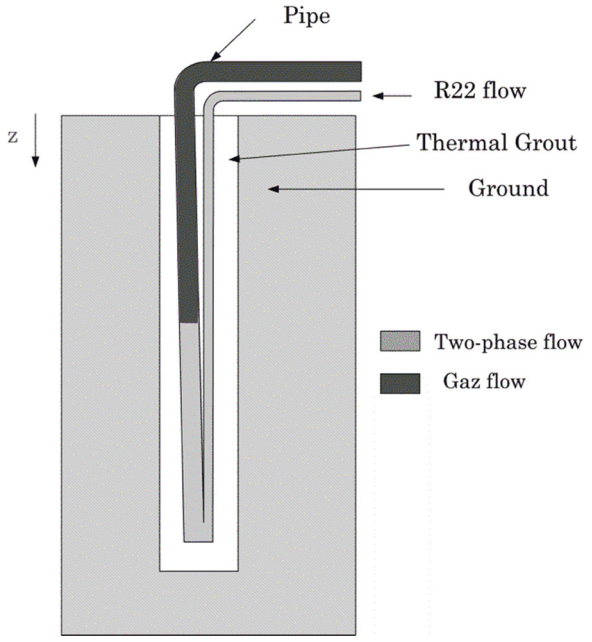

Fig. 2. Ground heat exchanger.

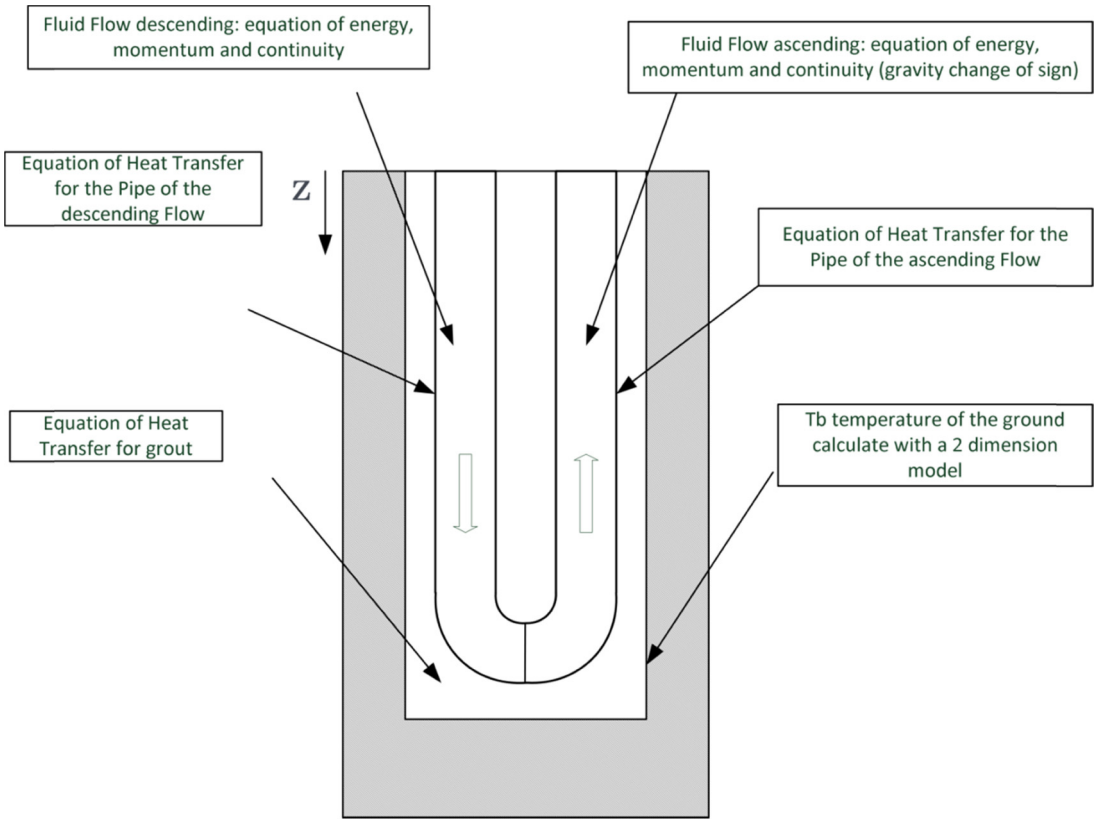

Fig. 3. Model.

- The grout, in one dimension (z);
- The ground, in two dimensions (x, y).

2.1. Flow of R22

For the R22, the homogeneous multiphase flow is used (Ishii, 1975), illustrated below in Eqs. (1)–(3) for the ascending flow and for the descending flow:

$$\frac{\partial \rho_m \cdot A}{\partial t} + \frac{\partial \dot{m}}{\partial z} = 0 \tag{1}$$

$$\frac{\partial \dot{m}}{\partial t} + \frac{\partial \dot{m} \cdot v}{\partial z} + \frac{\partial P_m \cdot A}{\partial z} = -\tau_w \cdot Pr - \rho \cdot A \cdot g \cdot \sin\theta \tag{2}$$

$$\frac{\partial \rho_m \cdot A \cdot h_m}{\partial t} + \frac{\partial \dot{m} \cdot h}{\partial z} = \frac{\partial P_m \cdot A}{\partial t} + q_r + v\frac{\partial P_m \cdot A}{\partial z} \tag{3}$$

The differences between the ascending and descending flows are:

- The sign of the gravity term which is negative for the descending flow and positive for the ascending flow.
- The addition of a pressure drop in the U-bend, at the entry of the ascending flow.

With

$$q_r = H_r \cdot \pi \cdot D_i \cdot (T_p - T) \tag{4}$$

$$\tau_w = \frac{f \cdot \dot{m} \cdot v}{8} \tag{5}$$

H_r in Eq. (4) is calculated with:

- Gnielinski (Gnielinski, 1975), Eq. (6) for one-phase flow;
- Chen (Chen, 1966) correlation, Eq. (7), for two-phase flow.

Gnielinski correlation:

$$H_r = \left(\frac{k_m}{D_i}\right)\left[\frac{\left(\frac{f}{8}\right)\cdot(Re-1000)\cdot Pr}{1+12.7\cdot\left(\frac{f}{8}\right)^{1/2}\cdot\left(Pr^{2/3}-1\right)}\right] \tag{6}$$

Chen correlation:

$$H_r = H_{mic} + H_{mac} \tag{7}$$

$$H_{mic} = 0.00122\cdot\left[\frac{k_f^{0.79}\cdot Cp_f^{0.45}\cdot\rho_f^{0.49}}{\sigma^{0.5}\cdot\mu_f^{0.29}\cdot h_{fg}^{0.24}\cdot\rho_g^{0.24}}\right][T_p - T_{sat}\cdot(P_m)]^{0.24} \tag{8}$$

$$[P_{sat}\cdot(T_p) - P_m]^{0.75}\cdot S$$

$$S = \frac{\left[1-\exp\left(-(F(X_{tt})\cdot H_f\cdot X_0)/k_f\right)\right]}{(F(X_{tt})\cdot H_f\cdot X_0)/k_f} \tag{9}$$

$$X_0 = 0.041\cdot\left[\frac{\sigma}{g\cdot(\rho_f-\rho_g)}\right]^{0.5} \tag{10}$$

$$X_{tt} = \left(\frac{1-x}{x}\right)^{0.9}\cdot\left(\frac{\rho_g}{\rho_f}\right)^{0.5}\cdot\left(\frac{\mu_f}{\mu_g}\right)^{0.1} \tag{11}$$

$$H_f = 0.023\cdot\left(\frac{k_f}{D_i}\right)\cdot Re_f^{0.8}\cdot Pr_f^{0.4} \tag{12}$$

$$Re_f = \frac{G\cdot(1-)\cdot D_i}{\mu_f} \tag{13}$$

$$H_{mac} = H_f\cdot F(X_{tt})\cdot Pr_f^{0.296} \tag{14}$$

$$F(X_{tt}) = 1 \text{ if } X_{tt}^{-1} \le 0.1 \tag{15}$$

$$F(X_{tt}) = 2.35\cdot\left(0.213+\frac{1}{X_{tt}}\right)^{0.736} \text{ if } X_{tt}^{-1} > 0.1 \tag{16}$$

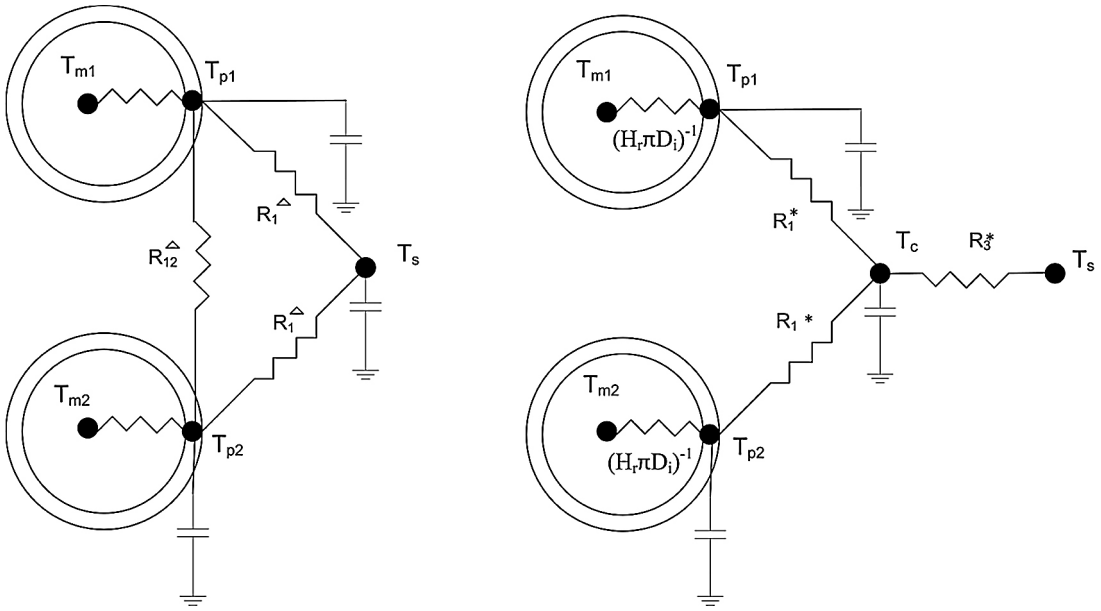

Fig. 4. Thermal resistances of the borehole.

The pressure drop in the case of the two-phase flow in the tube is calculated with the Müller-Steinhagen and Heck Correlation (Muller-Steinhagen and Heck, 1986), Eqs. (17)–(20). In the literature (ASHRAE Handbook – Fundamentals, 2009), deviations of 30–50% are common for all the correlations of pressure drop in a two-phase flow between models and measured pressure drops. Here, the Müller-Steinhagen and Heck correlation is increased by 55% in the model to match the measured pressure drop.

$$\frac{dp}{dz} = \Delta \cdot (1-x)^{1/3} + \left(\frac{\partial P}{\partial z}\right)_g \cdot x^3 \tag{17}$$

$$\Delta = \left(\frac{\partial P}{\partial z}\right)_f + 2 \cdot \left[\left(\frac{\partial P}{\partial z}\right)_g - \left(\frac{\partial P}{\partial z}\right)_f\right] \cdot x \tag{18}$$

$$\left(\frac{\partial P}{\partial z}\right)_f = f_f \cdot \frac{2 \cdot G_{tot}^2}{D_i \cdot \rho_f} \tag{19}$$

$$\left(\frac{\partial P}{\partial z}\right)_g = f_g \cdot \frac{2 \cdot G_{tot}^2}{D_i \cdot \rho_f} \tag{20}$$

For the pressure drop of the bend, the Domanski correlation (Domanski and Hermes, 2008) is used (Eqs. (21) and (22)). This correlation is obtained by multiplying the Müller-Steinhagen and Heck Correlation by a curvature correlation defined by Domanski:

$$\left[\frac{\partial P}{\partial z}\right]_{bend} = \left(\frac{\partial P}{\partial z}\right) \cdot \Lambda \tag{21}$$

$$\Lambda = a_0 \cdot \left(\frac{G_{tot} \cdot x \cdot D_i}{\mu_g}\right)^{a_1} \cdot \left(\frac{1}{x} - 1\right)^{a_2} \cdot \left(\frac{\rho_f}{\rho_g}\right)^{a_3} \cdot \left(\frac{2 \cdot R}{D_i}\right)^{a_4} \tag{22}$$

With a_0, a_1, a_2, a_3 and a_4 constant for the R22.

2.2. Pipe

The temperature of the pipe is solved with the following Eqs. (23) and (24):

$$\rho_p \cdot A_p \cdot Cp_p \frac{dT_p}{dt} = -q_r + q_p + k_p \cdot \frac{\partial^2 T_p}{\partial z^2} \tag{23}$$

$$q_p = H_p \cdot \pi \cdot D_e \cdot \left(T_c - T_p\right) = R_1^* \cdot \left(T_c - T_p\right) \tag{24}$$

The resistance R_1^* is calculated using the Kennelly's delta-star transformation of the circuit of Hellstrom (1991), Fig. 6. For more information about the star diagram, see (Beauchamp et al., 2013) (Fig. 4).

$$R_1^* = \frac{R_1^\Delta \cdot R_{12}^\Delta}{2 \cdot R_1^\Delta + R_{12}^\Delta} = \frac{1}{H_p \cdot \pi \cdot D_e} \tag{25}$$

$$R_3^* = \frac{\left(R_1^\Delta\right)^2}{2 \cdot R_1^\Delta + R_{12}^\Delta} = \frac{1}{H_s \cdot \pi \cdot D_b} \tag{26}$$

H_s and H_p was calculated with the Eqs. (25) and (26).

2.3. Grout

The temperature of the grout is solved with Eqs. (27) and (28):

$$\rho_c \cdot A_c \cdot Cp_c \cdot \frac{dT_c}{dt} = -q_{p1} - q_{p2} + q_s + k_c \cdot \frac{\partial^2 T_c}{\partial z^2} \tag{27}$$

$$q_s = H_s \cdot \pi \cdot D_b \cdot (T_s - T_c) \tag{28}$$

q_{p1} and q_{p2} are respectively the flux of the descending flow pipe and ascending flow pipe to the grout and Hs is calculated with Eq. (28).

2.4. Ground

The ground temperature is calculated with a two-dimensional model,

$$\rho_s \cdot Cp_s \cdot \frac{dT_s}{dt} = k_s \cdot \frac{\partial^2 T_s}{\partial x^2} + k_s \cdot \frac{\partial^2 T_s}{\partial y^2} \tag{29}$$

with at the contact between the ground and the borehole:

$$n \cdot (-k_s \cdot \nabla T_s) = H_s \cdot (T_{c_{mean}} - T_s) \tag{30}$$

The interest in using a two-dimensional model lies in the fact that it makes it possible to take into account the effect of a borehole to an over one. In this article, we study only one active borehole at a time, but in a more complex study, the position of boreholes relative to one another can easily be studied with this two-dimensional

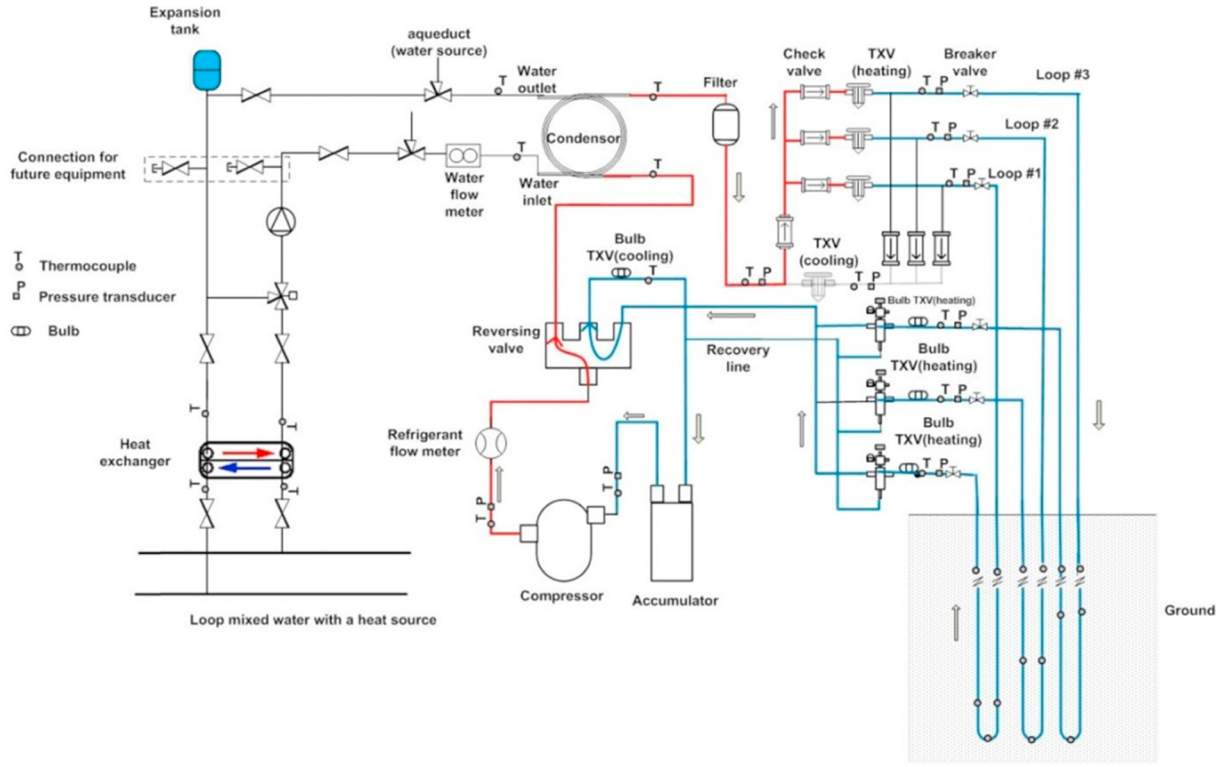

Fig. 5. Schematic of the experimental device in heating mode.

model. The model was compared to, and validated using a model developed by Lamarche (2011) of the ground.

3. Model

The model is compared to the experimental heat pump located at CTT in Montreal (Fig. 5), with only one loop activated.

The borehole is 30 m long, but the internal piping from the heat pump to the borehole is not insulated, so 10 m is added to take account the heat exchange of the refrigerant in this part (Fig. 6). The following measurements are carried out in the experiment: the pressure and the temperature before the valve, the mass flow rate at the exit of the compressor and the temperatures of the pipe at five different positions in the loop:

- $z = 10$ m in the descending flow;
- $z = 34$ m in the descending flow;
- $z = 40$ m in the U-bend;
- $z = 34$ m in the ascending flow;
- $z = 10$ m in the ascending flow.

In $z = 0$ m, the conditions at the entry of the evaporator for the descending flow are the flow rate and enthalpy.

The enthalpy is calculated with the pressure and the temperature of the pipe minus one degree before the valve. The temperature correction of one degree is the difference between the temperature of the pipe, which is measured, and the temperature of the R22, that we need for the calculation of the enthalpy.

For $z = 0$:

$$\dot{m}_1 = \dot{m}_i$$

$$h_m = h_i$$

The same condition is imposed for all z at $t = 0$.

In the experiment, the pressure at the entry is not measured. However, with the temperature of the pipe at $z = 10$ m, and with the hypothesis that the refrigerant is in a saturated mixture, the pressure can be calculated; this pressure is imposed at $z = 10$ m for the descending flow (Fig. 6).

$P_m = P_{sat}$ for $z = 10$ m

For $z = 40$ m for the ascending flow:

$$\dot{m}_2 = \dot{m}_1$$

$$P_{m2} = P_{m1} - \Delta P_{bend}$$

$$h_{m2} = h_{m1}$$

For more information on the experiment, see the experimental study by Fannou et al. (2014).

The boundary conditions for the 2D ground model are summarized in Fig. 7.

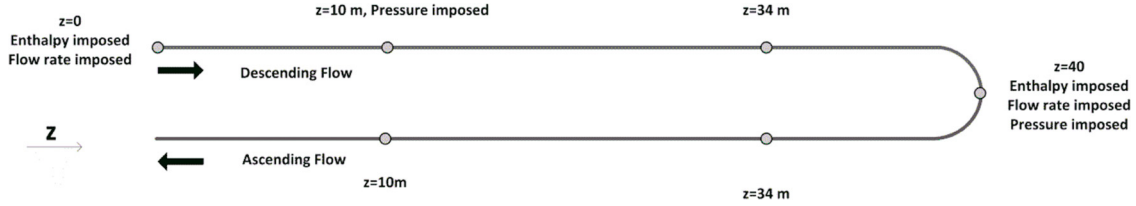

Fig. 6. Schematic of the borehole.

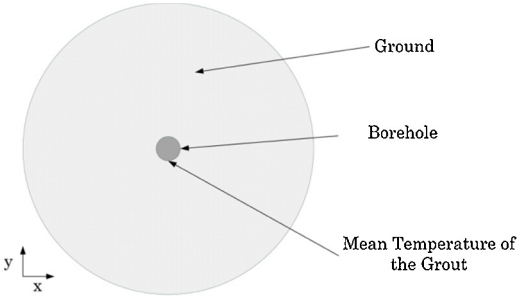

Fig. 7. Two-dimensional model of the ground.

All the properties of the fluid depend on the enthalpy and the pressure; they are obtained with the RefProp software.

4. Results

4.1. Validation

To validate the model, a comparison between the simulated and measured values of the temperature of the pipe in five different locations was carried out. A comparison is also done on the enthalpy and the pressure at the exit. We also performed a comparison with an experiment conducted in our laboratory in a 2-h test. As stated earlier, the entry of the model is the enthalpy and the mass flow rate at $z = 0$ m and the pressure at $z = 10$ m.

The measured pressure presented in Fig. 8 is seen to be highly oscillating. In order to avoid a small time step, only smoothed values are imposed in our model with a three-order polynomial equation.

The inlet enthalpy is show in Fig. 9.

The mass flow rate is measured at the exit of the compressor. Even if only one loop is activated, a small portion of the flow rate enters loops 2 and 3 (based on the result of the experiment). The flow rate is decreased by 20% to take this effect into account (Fig. 10).

The properties of the ground, grout and pipe are presented in Table 1.

Figs. 10–15 show the calculated and the smoothed measured temperature of the pipe at five different positions:

- $z = 10$ m in the descending flow, Fig. 11;
- $z = 34$ m in the descending flow, Fig. 12;
- $z = 40$ m in the U-bend, Fig. 13;

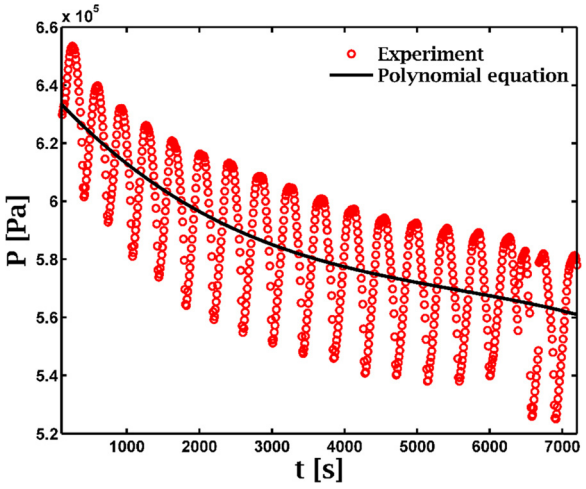

Fig. 8. Pressure at $z = 10$ m for descending flow.

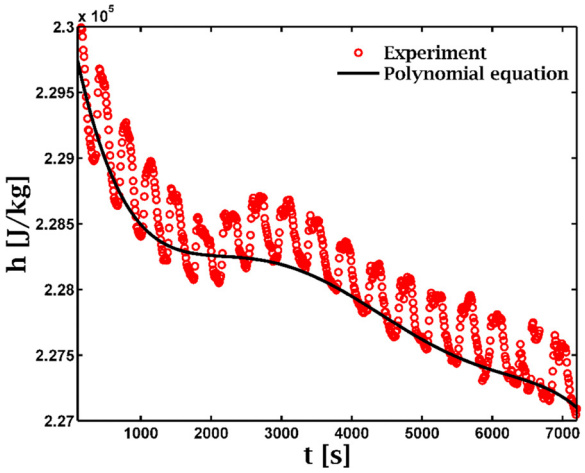

Fig. 9. Enthalpy at the entry of the evaporator.

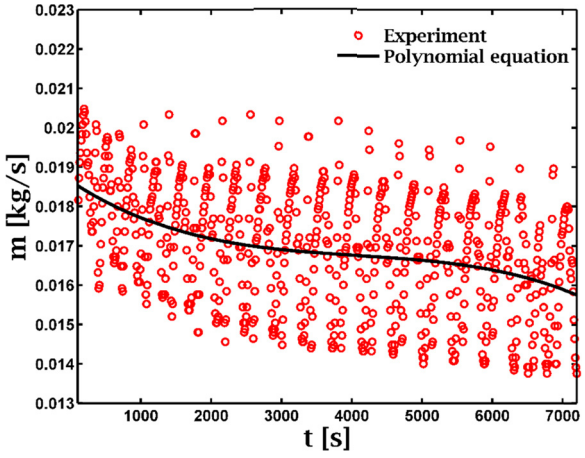

Fig. 10. Mass flow rate at the entry of the evaporator.

- $z = 34$ m in the ascending flow, Fig. 14;
- $z = 10$ m in the ascending flow, Fig. 15.

In all the figures, the evolution of the temperature is the same for the model and for the experiment. The difference at the beginning

Table 1
Parameters of the model.

Variables	Values
Le1, length of the descending flow (m)	40
Le2, length of the ascending flow (m)	40
Di1, internal diameter of descending flow (mm)	7.9
Di2, internal diameter of ascending flow (mm)	11.07
Di1, external diameter of descending flow (mm)	9.5
Di2, external diameter of ascending flow (mm)	12.7
T_s, initial temperature (K)	287.5
D_b, diameter of the borehole (m)	0.076
D, distance between pipes (m)	0.02
k_p (W/m K)	401
Cp_p (J/kg K)	385
ρ_p (kg/m^3)	1000
k_{grout} (W/m K)	1.6
Cp_{grout} (J/kg K)	800
ρ_{grout} (kg/m^3)	2300
k_{grout} (W/m K)	2.8
Cp_{grout} (J/kg K)	600
ρ_{grout} (kg/m^3)	2000
θ	$\frac{\pi}{2}$

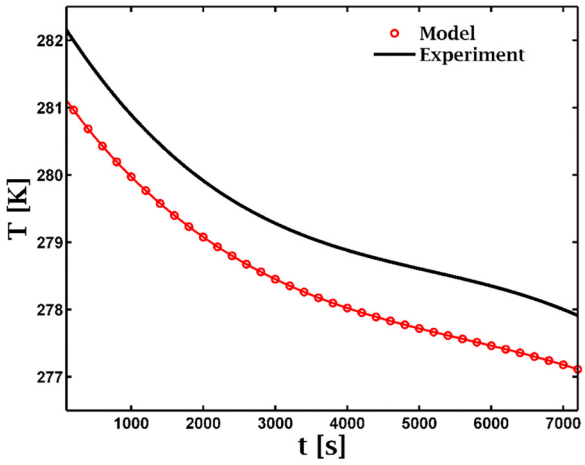

Fig. 11. Temperature at $z = 10$ m in the descending flow.

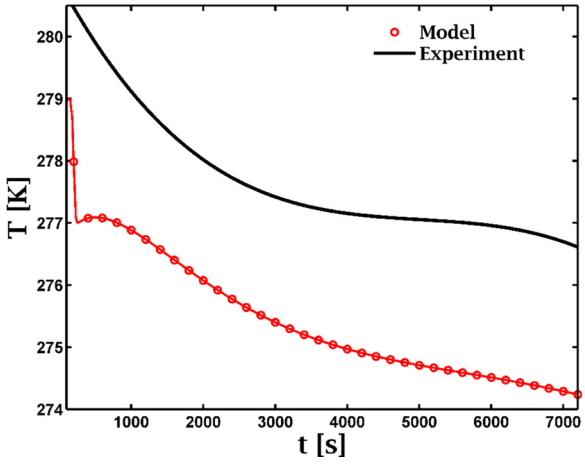

Fig. 12. Temperature at $z = 34$ m in the descending flow.

of the test for Figs. 14 and 15 can be explained by the fact that the initial condition of the grout may be different.

Fig. 16 shows the difference between the model at 1000 and 7200 s. The maximum difference is 4.5 K, which is an acceptable error if we take into account all the precision of the correlations of a two-phase model.

The pressure at the exit of the heat exchanger is shown in Fig. 17.

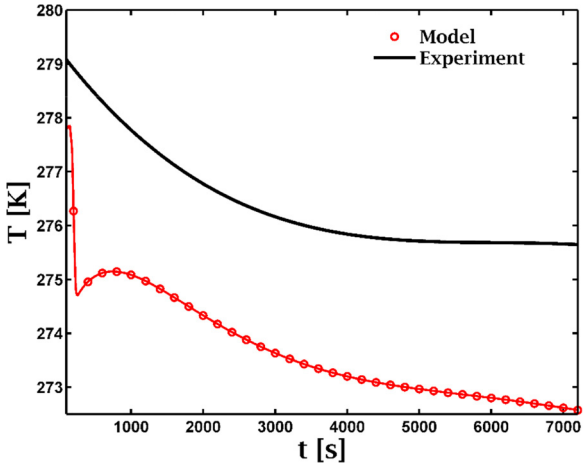

Fig. 13. Temperature at $z = 40$ m.

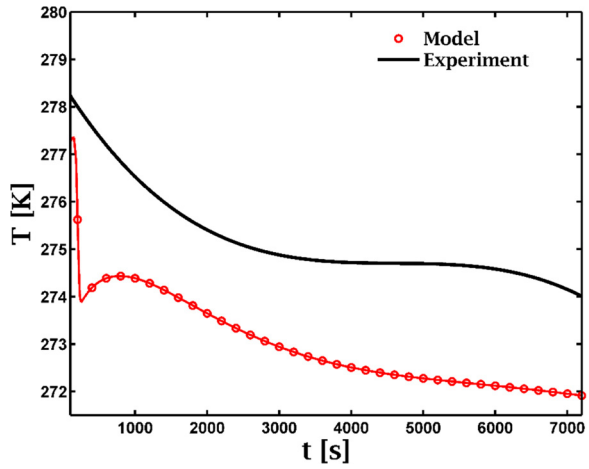

Fig. 14. Temperature at $z = 34$ m in the ascending flow.

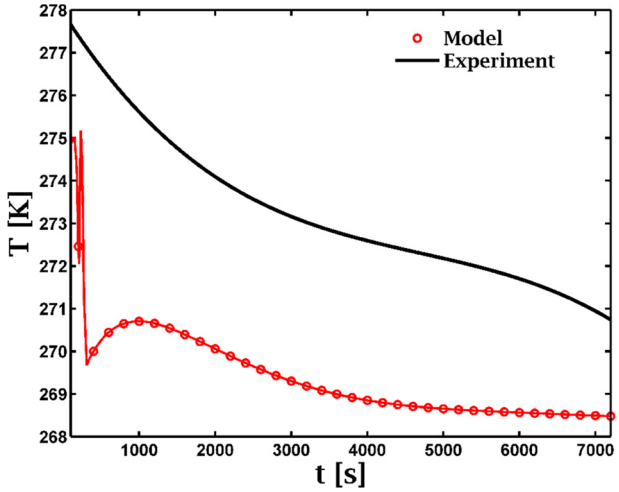

Fig. 15. Temperature at $z = 10$ m in the ascending flow.

In this figure, the experimental pressure is the measured pressure at the entry of the compressor. We do not have a real measure of the exit pressure of the heat exchanger in our experiment.

This partially explains the difference of approximately 150 kPa between these two pressures. It is also possible that the pressure

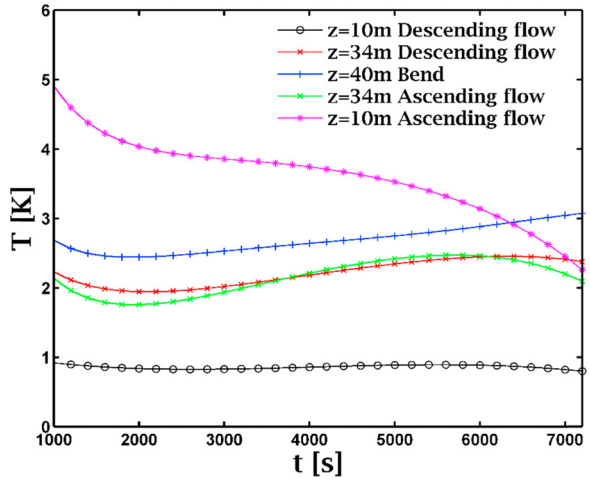

Fig. 16. Difference between the temperature of the pipe in the model and in the experiment.

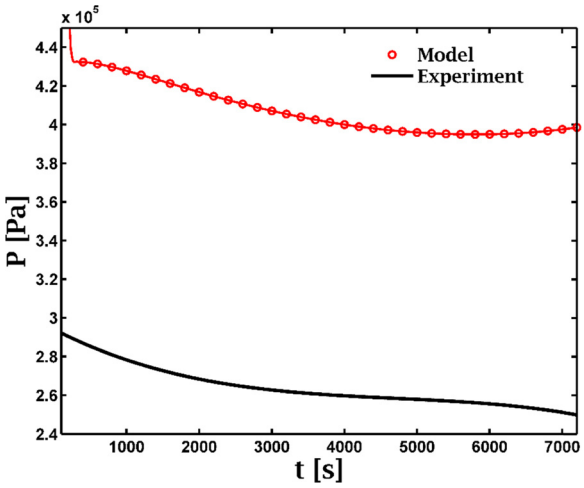

Fig. 17. Pressure at the exit of the exchanger.

drop in the exchanger was too low, even though it increased by 55%. This problem of the precision of the pressure drop correlation in a two-phase flow is frequently encountered in the literature.

Fig. 18 shows the difference between the calculated enthalpy at the exit of the heat exchanger and the measured value. We see that in this case, the correlation is better.

The superheat value at the exit of the evaporator calculated with the enthalpy and the pressure given in Fig. 17 −150 kPa (see previous comment) is presented in Fig. 19. We can see that the superheat is always present during the simulation.

Although some differences may be present, the complexity of the model and the precision of the correlations can partially explain this result. Even given this scenario, the difference is acceptable and represents a step toward a more complex model of a DX ground source heat pump.

4.2. Parametric study

Following this validation, a parametric study was realized to illustrate the importance of some parameters in the heat extraction rate of the exchanger.

The parameters are:

- The mass flow rate, Fig. 20;
- The length of the exchanger, Fig. 21;
- The angle of the borehole, Fig. 22.

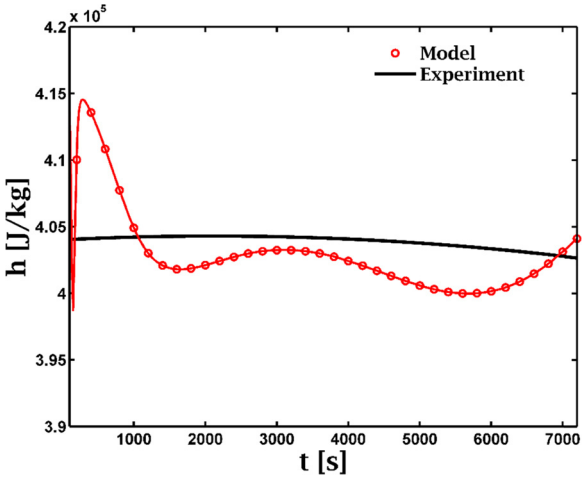

Fig. 18. Enthalpy at the exit of the exchanger.

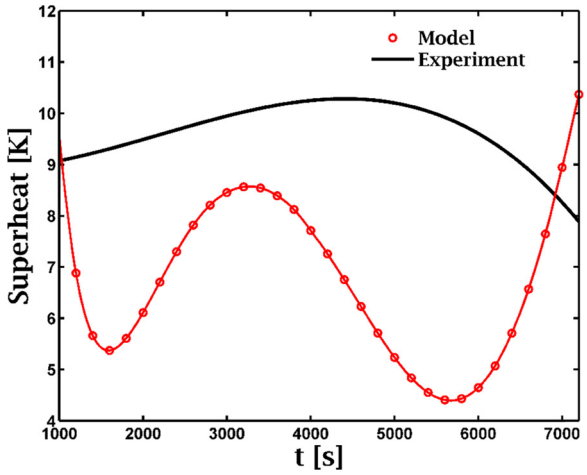

Fig. 19. Superheat.

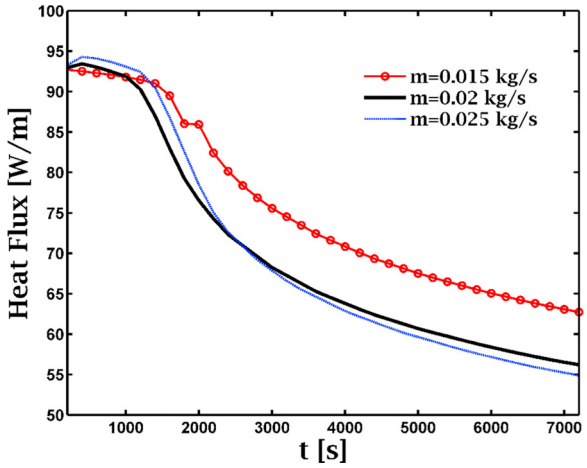

Fig. 20. Parametric study of the mass flow rate.

Fig. 20 shows the heat extraction rate in W/m with three different mass flow rates at the entry of the exchanger. At the beginning of the test, the heat flux is higher, with a higher mass flow rate (m = 0.025 kg/s), but after 2000 s, the inverse occurs. That can be explained by the fact that with a high mass flow rate, the temperature of the ground decreases quickly. It is then preferable, for the efficiency of the heat pump, to have more boreholes with smaller

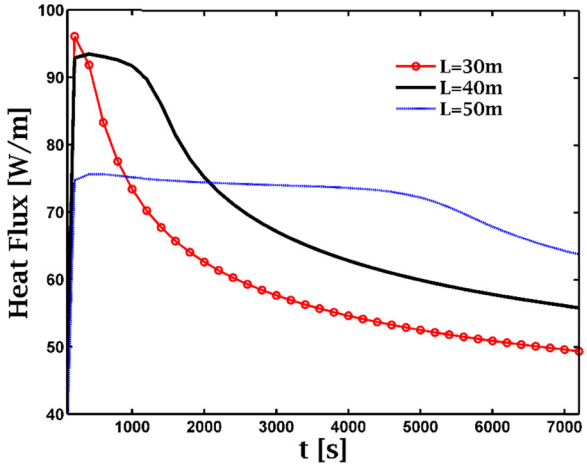

Fig. 21. Parametric study of the length of the borehole.

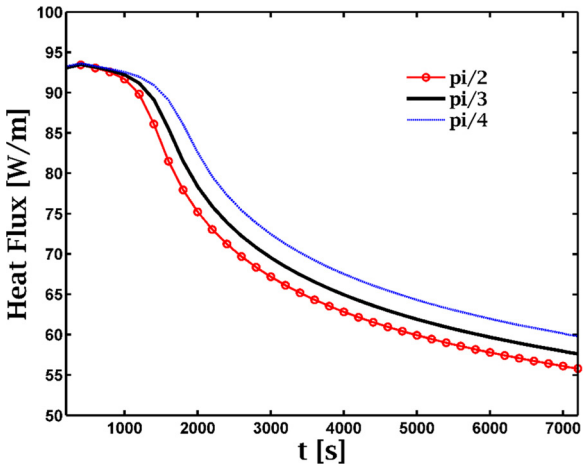

Fig. 22. Parametric study of the angle of the borehole.

mass flow rates than one with a high mass flow rate. Of course this remark does not take account the cost of drilling.

Fig. 21 shows that in a short period of time, the shorter borehole ($L = 30$ m) has the best efficiency of heat transfer by meter. This is because the phase changes occur across most of the exchanger length, and the heat flux is higher in a two-phase flow than in a one-phase flow. For example, at 1000 s, the phase change occurs on 100% of the length for 30 m, 90% for 40 m and 60% for 50 m.

This heat flux also decreases rapidly after a short period for $L = 30$ m, the same evolution happen at $L = 40$ m and $L = 50$ m but later. During the test, the ground temperature is decreasing and of course that will decrease the heat exchange between the R22 and the ground. This heat exchange is in two parts, the phase change with a big heat transfer coefficient (3000–5000 W/m^2 K) and the superheat with a small heat transfer coefficient (100–350 W/m^2 K). In the beginning of the test, the superheat decreases and the mean heat flux per meter does not change a lot. But when the superheat disappear the mean heat flux per meter decreases quickly because the phase change decreases. To conclude, for a constant and high heat flux per meter, a minimum superheat needs to be present.

Fig. 22 shows that the orientations have a direct impact on the heat flux of the heat exchanger. We can increase the heat exchange by 7% in 2 h by changing the angle of the borehole (compared to the horizontal) from $\pi/2$ to $\pi/4$. This can be explained by the fact that the pressure drop actually increases by 10% when the angle decreases. If the pressure is lower in the flow, the difference in temperature between the ground and the flow is higher and the heat flux increases. However, this increase in pressure drop is going to increase the work of the compressor, and thus decrease the performance of the global heat pump. Also, if the angle is too high, the cost of installation and the influence of the environment can increase. A more complex analysis needs to be done with a global model for this parameter.

This parametric analysis proves that for a higher heat extraction rate, the exchanger needs an optimum length, angle and a small mass flow.

5. Conclusion

Direct expansion (DX) ground source heat pump is an interesting technology for use in increasing the efficiency of building heating and cooling systems. A review of the literature reveals a dearth of scientific research on DX geothermal heat pump systems. To help design this technology, a model of a ground source heat pump needs to be developed. In this study, a model of the ground exchanger is presented for a heating process. The model represents the phase change of the refrigerant, here Chlorodifluoromethane R22, with governing continuity, momentum and energy equations and with a heat exchange between the pipe and grout and the grout and the ground. A comparison between the model and the experiment is performed. The results allow us to validate the model and to analyze the influence of the mass flow rate, the length of the exchanger and the angle between the borehole and the horizontal. The next step in improving the model is to link the model to other components, such as exchangers with water and a compressor, to have a complete model of the system, and to use it to improve the design of the ground heat exchanger for DX ground source heat pumps.

Acknowledgements

Financial support for this study was provided by the Natural Sciences and Engineering Research Council of Canada (NSERC), École de technologie supérieure, and its financial partners; the authors would like gratefully to acknowledge their invaluable contributions. In addition, the valuable comments of the reviewers are gratefully acknowledged.

References

ASHRAE Handbook – Fundamentals, 2009. American Society of Heating. Refrigerating and Air-Conditioning Engineers, Inc.
Beauchamp, B., Lamarche, L., Kajl, S., 2013. A numerical model of a U-tube vertical ground heat exchanger used as an evaporator. J. Energy Power Eng. 7, 237–249.
Capozza, A., De Carli, M., Zarrella, A., 2012. Design of borehole heat exchangers for ground-source heat pumps: a literature review, methodology comparison and analysis on the penalty temperature. Energy Build. 55, 369–379.
Chen, J.C., 1966. Correlation for boiling heat transfer to saturated fluids in convective flow. Ind. Eng. Chem. Process Des. Dev. 5 (3), 322–329.
Domanski, P.A., Hermes, C.J.L., 2008. An improved correlation for two-phase pressure drop of R-22 and R-410A in 180 return bends. Appl. Therm. Eng. 28 (7), 793–800.
Esen, H., Inalli, M., 2009. Modelling of a vertical ground coupled heat pump system by using artificial neural networks. Expert Syst. Appl. 36 (7), 10229–10238.
Fannou, J.-L., Rousseau, C., Lamarche, L., Kajl, S., 2014. Experimental analysis of a direct expansion geothermal heat pump in heating mode. Energy Build. 75, 290–300.
Freund, E.A., Whitlow, G.S., 1959. Earth source heat pumps: characteristics, design, and operation. Am. Inst. Electr. Eng. – Trans. Appl. Ind. 77 (40 (Pt 2)), 540–550.
Gnielinski, V., 1975. New equations for heat and mass transfer in the turbulent flow in pipes and channels. Forsch. Ing. 41 (1), 8.
Goulburn, J.R., Fearon, J., 1978. Deep ground coil evaporators for heat pumps. Appl. Energy 4 (4), 293–313.
Goulburn, J.R., Fearon, J., 1983. Domestic heat pump with deep hole ground source evaporator. Appl. Energy 14 (2), 99–113.
Halozan, H., 2011. Ground-Source Heat Pumps – Overcoming Market and Technical Barriers. IEA Heat Pump Programme.
Hellstrom, G., 1991. Ground Heat Storage, Thermal Analysis of Duct Storage Systems. Part I. Theory. University of Lund, Sweden.
Ishii, M., 1975. Thermo-Fluid Dynamic Theory of Two-Phase Flow. Eyrolles, Paris.
Lamarche, L., 2011. Analytical g-function for inclined boreholes in ground-source heat pump systems. Geothermics 40 (4), 241–249.
Muller-Steinhagen, H., Heck, K., 1986. A simple friction pressure drop correlation for two-phase flow in pipes. Chem. Eng. Process. 20 (6), 297–308.
Self, S.J., Reddy, B.V., Rosen, M.A., 2013. Geothermal heat pump systems: status review and comparison with other heating options. Appl. Energy 101, 341–348.
Smith, G.S., 1956. Intermittent ground grids for heat pumps. Heat. Pip. Air Cond. 28 (6), 127–133.
Wang, H., Zhao, Q., Wu, J., Yang, B., Chen, Z., 2013. Experimental investigation on the operation performance of a direct expansion ground source heat pump system for space heating. Energy Build. 61, 349–355.
Wang, X., Ma, C., Lu, Y., 2009. An experimental study of a direct expansion ground-coupled heat pump system in heating mode. Int. J. Energy Res. 33 (15), 1367–1383.